Altered immunolocalization of FGF23 in murine femora metastasized with human breast carcinoma MDA-MB-231 cells

Ayako Yokoyama[1,2], Tomoka Hasegawa[1§], Toru Hiraga[4], Tamaki Yamada[3], Yimin[5], Hiromi Hongo[1], Tomomaya Yamamoto[1,6], Miki Abe[1], Taiji Yoshida[1], Yasuo Imanishi[7], Shinichiro Kuroshima[8], Muneteru Sasaki[8], Paulo Henrique Luiz de Fraitas[9], Minqi Li[10], Norio Amizuka[1] and Yutaka Yamazaki[2]

[1]Developmental Biology of Hard Tissue, [2]Gerodontology, [3]Oral and Maxillofacial Surgery, Graduate School of Dental Medicine and Faculty of Dental Medicine, Hokkaido University, Sapporo, Japan, [4]Department of Oral Anatomy, Matsumoto Dental University, Shiojiri, Japan, [5]Central Research Institute, Graduate School of Medicine, Hokkaido University, Sapporo, Japan, Northern Army Medical Unit, Camp Makomanai, Japan Ground Self-Defense Forces, Sapporo, Japan, [7]Department of Nephrology, Osaka City University, Graduate School of Medicine, Osaka, Japan, [8]Department of Applied Prosthodontics, Unit of Translational Medicine, Graduate School of Biomedical Sciences, Nagasaki University, Nagasaki, Japan, [9]Department of Dentistry, Federal University of Sergipe at Lagarto, Brazil, [10]Division of Basic Science of Stomatology, The School of Stomatology, Shandong University, Jinan, China.

Running title: *FGF23 in metastasized bone*

§ Address for correspondence to

Tomoka Hasegawa DDS, PhD.
Developmental Biology of Hard Tissue,
Graduate School of Dental Medicine and Faculty of Dental Medicine,
Hokkaido University
Kita-13, Nishi-7, Kita-Ku, Sapporo, Japan
Tel/Fax: +81-11-706-4226
E-mail: hasegawa@den.hokudai.ac.jp

Abstract

After the onset of bone metastasis, tumor cells appear to modify surrounding microenvironments for their benefit, and particularly, the levels of circulating fibroblast growth factor (FGF) 23 in patients with tumors has been highlighted. Herein, we have attempted to verify if human breast carcinoma MDA-MB-231 cells metastasized in the long bone of nu/nu mice would synthesize FGF23. Serum concentrations of calcium, phosphate (Pi) and FGF23 were measured in control nu/nu mice, bone-metastasized mice, and mice with mammary gland injected with MDA-MB-231 cells mimicking primary mammary tumors. Consequently, MDA-MB-231 cells revealed intense FGF23 reactivity in metastasized lesions, whereas MDA-MB-231 cells cultured *in vitro* or when injected into the mammary glands (without bone metastasis) showed weak FGF23 immunoreactivity. Although the bone-metastasized MDA-MB-231 cells abundantly synthesized FGF23, osteocytes adjacent to the FGF23-immunopositive tumors, unlike intact osteocytes, showed no FGF23. Despite significantly elevated serum FGF23 levels in bone-metastasized mice, there was no significant decrease in the serum Pi concentration when compared with the intact mice and mice with a mass of MDA-MB-231 cells in mammary glands. The metastasized femora showed increased expression and FGFR1 immunoreactivity in fibroblastic stromal cells, whereas femora of control mice showed no obvious FGFR1 immunoreactivity. Taken together, it seems likely that MDA-MB-231 cells synthesize FGF23 when metastasized to a bone, and thus affect FGFR1-positive stromal cells in the metastasized tumor nest in a paracrine manner.

225 words

Key words: *fibroblast growth factor 23, osteocyte, immunohistochemistry, bone metastasis, MDA-MB-231*

Introduction

Bone metastasis is a critical condition in patients suffering from a malignant tumor and induces osteolytic, osteogenic, or combined lesions depending on the interaction between tumor cells and bone cells. Animal models mimicking bone metastasis in humans have been established to elucidate the intrinsic pathological events of bone metastasis using cancer cell lines: MDA-MB-231 cells of human breast carcinoma selectively colonize the femur and tibia of nu/nu mice, thus inducing osteolytic metastasis [1-5].

Among the various adverse events associated with osteolytic metastasis, such as bone pain, numbness, paralysis, bone fractures, and hypercalcemia, hypercalcemia is well known to worsen the patient condition by inducing nausea, vomiting, and consciousness disorder [6]. Tumor-induced osteomalacia/hypophosphatemia (TIO) is reportedly an adverse event caused by long-lasting secretion of fibroblast growth factor 23 (FGF23) from the tumors [7-14]. In TIO, FGF23-secreting tumors are typically present in patients; however, these tumors are often small, slow-growing, and benign with mesenchymal origin [12, 13]. Despite being pathologically different from TIO, malignant tumors metastasized to bone may synthesize FGF23. It is important to clarify if malignant tumors can secrete FGF23 when the tumor metastasizes to the bone.

In a normal state, FGF23 is mainly synthesized by osteocytes in adults [15, 16] and is circulated to reach the kidney. FGF23 binds the receptor complex of

FGFR1c/αklotho in proximal renal tubules to inhibit phosphate reabsorption of sodium phosphate by mediating co-transporter type IIa/IIc, consequently reducing the serum concentration of inorganic phosphate (Pi) [17-21].

In this context, the following aspects seem of particular interest: 1) whether malignant tumors could begin to secrete abundant FGF23 when metastasized to bone, 2) and if so, whether the secreted FGF23 by the tumors would affect the systemic level of serum Pi or would influence tumor cells themselves in the metastasized lesion. It is also of importance to clarify whether it is systemic hypophosphatemia or elevated FGF23 that is beneficial for tumor proliferation, matrix degradation, and surrounding tissue invasion.

Therefore, this study was designated to examine if metastasized human breast carcinoma MDA-MB-231 cells synthesize FGF23.

Materials and Methods

Tissue preparation for histological examination

All animal experiments were conducted under the Guidelines for Animal Experimentation of Hokkaido University (Approval No.16-0031). Human breast carcinoma MDA-MB-231 cells (American Type Culture Collection, Rockville, MD) were cultured in α-minimum essential medium (αMEM; Flow Laboratories, Irvine, Scotland) supplemented with heat-inactivated 10% fetal bovine serum (FBS; Cosmo Bio. Co. Ltd., Tokyo, Japan) at 37° C in a humidified atmosphere of 5% CO_2. As previously reported [2, 3, 5], MDA-MB-231 cells (10^5 cells per mouse) were injected into the left cardiac ventricle of 5-6 week-old BALB/c nu/nu mice (CLEA Japan Co. Ltd, Tokyo)

using a 22-gauge needle; the mice were anesthetized with an intraperitoneal injection of sodium pentobarbital (n=12). The same quantity of MDA-MB-231 cells was subcutaneously injected in the region of mammary glands of age-matched BALB/c nu/nu mice (n=12). For control experiments, only Ringer's solution was injected into the left cardiac ventricle (n=12). After 4 weeks, the femora of the treated mice were taken for soft X-ray examination (SOFRON Ltd, Tokyo, Japan). The body weight of the control mice and metastasized mice was measured (n=6 in each group). The nu/nu mice with bone metastasis, those having developed tumor mass in the mammary glands, and control mice were anesthetized with an intraperitoneal injection of sodium pentobarbital, and their blood samples were collected through cardiac ventricles to measure the concentrations of serum calcium (Ca), Pi, and FGF23. Thereafter, the mice were perfused with 4% paraformaldehyde diluted in 0.1 M phosphate buffer (pH 7.4), and the femora were removed and immersed in the same fixative for 24 h at 4 ℃ for histochemical examination [22, 23]. The femora were then decalcified with 10% ethylenediamine tetraacetic disodium salt (EDTA-2Na) solution and dehydrated with increasing concentrations of ethanol before paraffin embedding, whereas the specimens obtained from tumor-injected mammary glands were dehydrated before paraffin embedding without decalcification.

Immunohistochemistry for dentin matrix protein-1 (DMP-1), FGF23, FGFR1, and αklotho in the metastatic lesion

After the inhibition of endogenous peroxidase activity with methanol containing 0.3 % hydrogen peroxidase for 30 min, dewaxed paraffin sections were pretreated with 1% bovine serum albumin (BSA; Seologicals Proteins Inc. Kankakee, IL) in PBS (1% BSA-

PBS) for 30 min. The histological sections were then incubated with either rabbit antibody against DMP-1 (No. M176, Takara Bio Inc., Otsu, Japan) at a dilution of 1: 500 overnight at 4 °C, then, they were reacted with horseradish peroxidase (HRP)-conjugated swine anti-rabbit IgG (No. P0399, DakoCytomation, Glostrup, Denmark) at a dilution of 1: 100 for 1 h. Regarding the FGF23/FGFR1/αklotho axis, the histological sections were incubated with rat anti-FGF23 (No. MAB26291, R&D systems, Inc., Minneapolis, MN) at a dilution of 1: 100 for 2 h, and then, they were reacted with HRP-conjugated rabbit anti-rat IgG (No. A18921, Thermo Fisher Scientific, Inc., Waltham, MA). For the detection of FGFR1 and αklotho, the sections were incubated with mouse monoclonal anti-FGFR1 (No. ab824, Abcam plc., Cambridge, UK) at a dilution of 1: 25 or mouse monoclonal anti-mouse klotho antibody (No. KL11-A, Thermo Fisher Scientific Ltd., Waitham, MA) at a dilution of 1: 50 for 2 h. These sections were then reacted with HRP-conjugated rabbit anti-mouse IgG (No. 61-6520, Invitrogen Co., Camarillo, CA) at a dilution of 1: 100 for 1 h. For visualizing all immunoreactions, diaminobenzidine tetrahydrochloride (DAB) was used as the substrate. All sections were counterstained with methyl green and observed under a light microscope (Eclipse E800, Nikon Instruments Inc. Tokyo, Japan).

Double detection of tartrate-resistant acid phosphatase (TRAP) and osteopontin

After the treatment with 0.3 % hydrogen peroxidase and 1% BSA-PBS, the sections were incubated with rabbit anti-osteopontin antisera (No. LB-4225, Cosmo Bio, Co., Ltd., Tokyo, Japan) at a dilution of 1: 2000 for 1 h, followed by incubation with HRP-conjugated swine anti-rabbit IgG (DakoCytomation). The immunoreacted sections were subjected to the detection of TRAP enzymatic activity as previously described [22].

Briefly, slides were rinsed with PBS and incubated in a mixture of 2.5 mg of naphthol AS-BI phosphate (Sigma-Aldrich Co. LLC, St. Louis, MS), 18 mg of Red Violet LB (Sigma-Aldrich) salt, and 100-mM L (+)-tartaric acid (0.76 g, Nacalai Tesque, Inc., Kyoto, Japan) diluted in 30 mL of 0.1 M sodium acetate buffer (pH 5.0) for 15 min at 37 °C.

Immunocytochemistry of FGF23, FGFR1 and αKlotho on cultured MDA-MB-231 cells

MDA-MB-231 cells were cultured on glass coverslips in dishes with 3.5-cm diameter containing αMEM supplemented with heat-inactivated 10% FBS before immunocytochemistry of FGF23, FGFR1 and αklotho. The specimens were fixed with 4% paraformaldehyde in 0.1 M phosphate buffer (pH 7.4) for 2 h at RT. The specimens were rinsed with PBS several times and then treated with 1% BSA-PBS for 10 min. They were then incubated with rat anti-FGF23 (R&D systems) at a dilution of 1: 100 for 2 h and then with HRP-conjugated rabbit anti-rat IgG at a dilution of 1: 100 for 1 h. For the detection of FGFR1 and αklotho, the specimens were incubated with mouse anti-FGFR1 (Abcam PLC) at a dilution of 1: 25 or mouse anti-mouse klotho antibody (Thermo Fisher Scientific Ltd.) at a dilution of 1: 50 for 2 h. These sections were then reacted with HRP-conjugated rabbit anti-mouse IgG (Invitrogen Co. A) at a dilution of 1: 100 for 1 h. For visualizing the immunoreaction, DAB was used as the substrate, and the specimens were faintly counterstained with methyl green before observation under a light microscope.

Immunoblotting of FGF23 in control and metastasized femora

The femora obtained from control mice or mice metastasized with MDA-MB-231 were

extracted after euthanasia with an intraperitoneal injection of sodium pentobarbital. To prepare femur protein, the femora were frozen for storage, and then ground to a fine powder using a mortar and pestle cooled in liquid nitrogen. Protein from the powdered femora was lysed using RIPA buffer (FUJIFILM Wako Pure Chemical Corporation, Osaka, Japan) and collected after centrifugation at 4 °C (13000 rpm, 30 min). Total protein was quantified using the Pierce BCA Protein Assay Kit (Thermo Fisher Scientific Inc., Waltham, MA) and denatured by boiling at 100 °C for 5 min in 5× sample buffer. The same amount of total protein in each sample was separated with 10% Mini-Protean TGX gels (Bio-Rad Laboratories, Inc., Hercules, CA) and electrophoretically transferred onto polyvinylidene difluoride (PVDF) membranes (Bio-Rad Laboratories, Inc., Hercules, CA). After blocking with 2% BSA (Sigma-Aldrich, St. Louis, MO) in Tris-buffered saline with Tween 20 (TBS-T) for 1 h at RT, the membranes were incubated with FGF23 primary antibody (product no. MAB26291, R&D systems, Inc., Minneapolis, MN) at 1:600 dilution in 2% BSA in TBS-T at 4 °C overnight. Thereafter, the membranes were incubated with HRP-conjugated anti-rat secondary antibody (Thermo Fisher Scientific, Inc.) at 1:10000 for 1 h at RT. After washing, antigen–antibody complexes were visualized with ECL Prime Western Blotting Detection Reagent (GE Healthcare Life Sciences Inc., Chicago, IL). Image capture and analysis were performed using ImageQuant LAS 4000 (GE Healthcare Life Sciences Inc.) and ImageQuant TL version 8.1 (Cytiva, Tokyo, Japan). To normalize the signal intensity of FGF23 protein, we performed the Coomassie brilliant blue gel staining for total protein according to Hu et al. [24] and Nie et al. [25]. The same amount of total protein in each sample was separated with 10% Mini-Protean TGX gels, and then incubated in Coomassie brilliant blue solution (CBB, 0.1% R2350, 25% isopropanol, 10% acetic acid) for 45 min. They were

then de-stained using the de-stain solution (10% acetic acid, 7% ethanol) overnight. Lastly, the stained gels were washed with distilled water and captured using ImageQuant LAS 4000 (GE Healthcare Life Sciences Inc.) and ImageQuant TL version 8.1 (Cytiva, Tokyo, Japan). The results of the normalized FGF23 protein are presented as the relative protein expression. The fold-change in FGF23 protein expression relative to the control was calculated using ImageQuant TL version 8.1.

Measurement of serum FGF23, Ca, Pi, intact PTH, 1α,25(OH)$_2$D$_3$, and CRE

Blood samples were obtained from all mice: control mice, mice metastasized with MDA-MB-231, and mice bearing MDA-MB-231 in the regions of the mammary glands (n=6 each), as previously reported [26]. Serum samples were stored at −30 °C before assaying. Serum levels of Ca, Pi, intact PTH, 1α,25(OH)$_2$D$_3$, and creatinine (CRE) were quantified by Oriental Yeast Co., Ltd. Serum intact FGF23 was quantified using sandwich ELISA kits (Kainos Laboratories, Tokyo, Japan) as previously reported [27]. All assays were performed in accordance with the manufacturers' instructions.

Statistical analysis

Statistical analyses on the serum concentration of FGF23, Pi, and calcium were assessed using one-way ANOVA followed by the Tukey-Kramer multiple comparisons test as reported previously [26], whereas statistical analyses on the serum concentration of intact PTH, 1α,25(OH)$_2$D$_3$, and CRE, the quantified image of mRNA expression of FGF23, FGFR1, and αklotho, and the quantified image of protein expression of FGF23 were conducted using Student's *t-te*st. All values are presented as mean ± SE (standard error). Values of $P < 0.05$ were considered statistically significant.

RT-PCR and real-time PCR for the expression of Fgf 23, Fgfr1, αKlotho, and Gapdh in the femora and mammary glands

To evaluate the mRNAs encoding *Fgf23, Fgfr1, αKlotho,* and *Gapdh*, total RNA was extracted from the femora of control mice, the femora of mice metastasized with MDA-MB-231 cells, the mammary glands of control mice, and mammary glands injected with MDA-MB-231 cells, as previously reported [16]. In brief, the metastasized femora were sagitally cut, and the bone-metastasized tumor nests inside the femora were confirmed under a binocular microscope and then extracted from the femora. The control femora and metastasized MDA-MB-231 cells in the femora, as well as the control and MDA-MB-231 cell-injected mammary glands were homogenized in 10 mL of TRIzol reagent (Life Technologies Co., Carlsbad, CA) per 1 g of tissue to extract total RNA. The obtained RNA pellet was washed with 1 mL of 75% ethanol, briefly air-dried, and then dissolved in DEPC-treated water. First-strand cDNA was synthesized from 2 μg of total RNA using a SuperScript VlLO cDNA Synthesis Kit (Life Technologies).

The primer sequences were as follows:

mouse *Gapdh*	Forward	TGTCTTCACCACCATGGAGAAGG
	Reverse	GTGGATGCAGGGATGATGTTCTG
mouse *Fgf23*	Forward	TGTCAGATTTCAAACTCAG
	Reverse	GGATAGGCTCTAGCAGTG
mouse *Fgfr1*	Forward	CTTGACGTCGTGGAACGATCT
	Reverse	AGAACGGTCAACCATGCAGAG
mouse *αKlotho*	Forward	TGGCTTTCCTCCTTTAC
	Reverse	AGGTTTGCGTAGTCT

The PCR was performed using a thermal cycler as follows: denaturation at 94 °C for 30 s, annealing at 60 °C (for *Gapdh*) or 55 °C (for *Fgf23*, *Fgfr1c*, and *αKlotho*) for 30 s, extension at 72 °C for 30 s, and a final incubation at 72 °C for 10 min. RT-PCR products were subjected to 1.5% agarose gel electrophoresis, stained with ethidium bromide, and detected using an E-Gel Imager (Life Technologies). Real-time PCR assays were performed using Taqman probes (Applied Biosystems) for the gene expression of *Fgf23* (Mm00445621_m1), *Fgfr1* (Mm00438930_m1), and *αKlotho* (Mm00502002_m1). Gene expression was detected using the StepOne Real-Time PCR System (Applied Biosystems), and levels were normalized to Gapdh (Mm99999915_g1) expression. The results are presented as the relative gene expression. The fold-change in gene expression relative to the control was calculated using the 2ΔΔCt method with StepOne Real-Time PCR System Software v2.2.2.

Results

Osteolytic bone metastasis by MDA-MB-231 cells

After 4 weeks, the average body weight of the control mice was 20.3 ± 0.3 g and that of the metastasized mice was 15.6 ± 0.5 g, showing a significant difference ($p<0.001$). Soft X-ray analysis revealed broad translucent areas representing metastatic lesions in the metaphyses of both the left and right femora and tibiae of nu/nu mice **(Fig. 1a)**. Consistent with the findings of soft X-ray analysis, histological observation revealed huge masses of metastasized MDA-MB-231 cells in the femoral metaphyses **(Fig. 1b)**. The metastasized tumor nests had a higher cell density than the surrounding bone marrow.

Inside the metastasized lesion, there were only a few fragmented trabeculae featuring intense osteopontin-reactive lines and many TRAP-positive osteoclasts, indicating osteolytic lesion **(Fig. 1c** and **d)**.

Immunolocalization of FGF23 in MDA-MB-231 cells and osteocytes in bone of the metastasized lesion

The cultured MDA-MB-231 cells showed very weak FGF23 immunoreactivity *in vitro* as shown in **Fig. 5g**. However, after the onset of bone metastasis, MDA-MB-231 cells metastasized in the femoral metaphyses demonstrated markedly intense FGF23 immunoreactivity **(Fig. 2a)**. The osteocytes in metaphyseal trabeculae surrounded by the metastasized MDA-MB-231 cells showed no FGF23 immunoreactivity, whereas those in trabeculae distant from the metastatic lesion showed FGF23-immmunopositivity **(Compare Fig. 2b** and **c)**. Western blotting coincidently demonstrated an intense band of 32-kDa full-length FGF23 in the metastasized femora, compared to the control specimens **(Fig. 2d)**. Image capture and analysis revealed that the index of FGF23 protein expression normalized by the total protein intensity **(Fig. 2f** and **g)** was 1.00 ± 0.15 in the control femora and 3.58 ± 0.38 in the metastasized femora (n=6 for each, $p<0.001$) **(Fig. 2e)**. Likely, osteocytes in the diaphyseal cortical bone adjacent to the metastasized tumor nests showed no FGF23 immunoreactivity, whereas those distant from the metastatic lesion showed intense FGF23 immunoreactivity **(Fig. 3a, Compare 3c** and **e)**. Despite the disappearance of FGF23 in osteocytes adjacent to the metastasized tumors, DMP-1, another osteocyte-derived molecule, was abundantly expressed in osteocytes in the cortical bone adjacent to the metastasized tumor nests **(Fig. 3b, See 3d** and **f)**, suggesting that osteocytes close to the metastasized tumor cells were

inhibited to synthesize FGF23 but not DMP-1.

Serum concentration of FGF23, Ca, Pi, intact PTH, 1α,25(OH)$_2$D$_3$, and CRE in mice

Mice with bone metastasis showed significantly higher serum FGF23 levels than those bearing mammary glands with MDA-MB-231 cell injection (386 ± 59 pg/mL vs. 230 ± 9 pg/mL, $p < 0.05$) and control mice without injection of tumor cells (386 ± 59 pg/mL vs. 156 ± 18 pg/mL, $p < 0.01$) **(Fig. 4a)**. Despite the increased concentration of serum FGF23, there was no significant difference in serum Pi levels among mice with bone metastasis (8.30 ± 0.58 mg/dL), mice with subcutaneous tumor injection in mammary glands (8.62 ± 0.61 mg/dL), and control mice (8.20 ± 0.46 mg/dL) **(Fig. 4b)**. Similarly, there was no significant difference in serum Ca levels among mice with bone metastasis (7.90 ± 0.22 mg/dL), mice with subcutaneous tumor injection in mammary glands (8.36 ± 0.26 mg/dL), and control mice (7.82 ± 0.13 mg/dL) **(Fig. 4c)**. However, all levels of intact PTH and 1α,25(OH)$_2$D$_3$ were reduced in the metastasized mice compared with the control mice, all showing significant differences **(Fig. 4d** and **e)**. The concentration of intact PTH was 169.0 ± 50.2 pg/mL for control mice and 35.4 ± 4.2 pg/mL for metastasized mice ($p<0.001$, **Fig. 4d**); the concentration of 1α,25(OH)$_2$D$_3$ was 18.6 ± 1.4 pg/mL in control mice and 10.1 ± 1.8 pg/mL in metastasized mice ($p<0.01$, **Fig. 4e**). In contrast, CRE was significantly increased in the metastasized mice (0.155 ± 0.032 mg/dL) compared with the control mice (0.084 ± 0.006 mg/dL) ($p<0.05$, **Fig. 4f**).

The immunolocalization of FGFR1 and αklotho in the metastasized femora and mammary glands injected with MDA-MB-231 cells

Since bone-metastasized MDA-MB-231 cells did not affect the serum concentration of

Pi, we examined the possibility that FGF23 secreted by tumor cells affects the cells themselves by mediating its receptor. Consequently, FGFR1 immunoreactivity was observed in fibroblastic stromal cells that extended their cytoplasmic processes in the metastasized lesion **(Fig. 5a** and **b)**. Some fibroblastic stromal cells in tumor nests also showed weak immunoreactivity of αklotho **(Fig. 5c)**. In order to verify whether the synthesis of αklotho and FGFR1 of MDA-MB-231 cells is affected by bone metastasis, we additionally examined the immunolocalization of αklotho and FGFR1 in cultured MDA-MB-231 cells and in the tumor nests of MDA-MB-231 subcutaneously injected into the mammary glands **(Fig. 5d-i)**. The tumor nests containing large amounts of MDA-MB-231 cells in the mammary glands demonstrated weak FGF23 **(Fig. 5d)** and FGFR1 **(Fig. 5e)** expression, but no αklotho **(Fig. 5f)**. Cultured MDA-MB-231 cells did not show obvious immunoreactivity of αklotho **(Fig. 5i)** or FGFR1 **(Fig. 5h)**.

Gene expression of Fgf23, Fgfr1 and αKlotho in the control and metastasized femora and control and MDA-MB-231 cell-injected mammary glands

Both RT-PCR and real-time PCR demonstrated the elevated expression of *Fgfr1* in the metastasized femora compared to the control femora. The relative expression ratio was 1.00 ± 0.03 in the control femora and 2.16 ± 0.09 in the metastasized femora ($p<0.001$). However, there was no significant difference in *Fgf23* and *αklotho* expression between the control and metastasized femora (**Fig. 6a** and **b**). In contrast, there was no significant difference in *Fgf23* expression between the control and the MDA-MB-231 cell-injected mammary glands (**Fig. 6c** and **d**). However, genes encoding *Fgfr1* and αklotho were markedly reduced in mammary glands injected with MDA-MB-231 cells (*Fgfr1*: 1.00 ± 0.08 in control mammary glands and 0.66 ± 0.04 in mammary glands

injected with MDA-MB-231 cells, $p<0.01$; *αklotho*: 1.00 ± 0.16 in control mammary glands and 0.00 ± 0.00 in mammary glands injected with MDA-MB-231 cells, $p<0.001$).

Discussion

This study shows that 1) MDA-MB-231 cells synthesized FGF23 when metastasized to a bone, even though they did not produce FGF23 in other conditions, such as in cell culture or when injected into mammary glands; 2) osteocytes were inhibited from synthesizing FGF23 when closely surrounded by FGF23-secreting MDA-MB-231 cells, while osteocytes apart from MDA-MB-231 cells synthesized FGF23; 3) despite highly-elevated serum concentrations of FGF23, there was no significant change in the serum concentration of Pi, while the serum levels of intact PTH and $1\alpha,25(OH)_2D_3$ were significantly reduced and the concentration of serum CRE was elevated in mice with bone metastases; 4) consistent with the elevated expression of the *Fgfr1* gene, intense FGFR1 immunoreactivity was observed in fibroblastic stromal cells in metastasized tumor nests; and 5) the metastasized femora demonstrated a comparable expression of klotho gene compared to the control femora. Taken together, we can hypothesize that MDA-MB-231 cells synthesize FGF23 when metastasized to a bone, presumably not only systemically affecting the serum Pi concentration in the kidney but also permitting the tumor-derived FGF23 to affect the FGFR1-positive stromal cells in a paracrine manner in the tumor nest.

This may raise a question of how and why MDA-MB-231 cells acquired to synthesize FGF23 after the onset of bone metastasis. There are several reports on the regulation of

FGF23 expression in various states: pro-inflammatory stimuli are reportedly capable of increasing osteocytic secretion of FGF23 [28]; insulin suppresses the FGF23 production [29]; the disrupted function of neurofibromatosis type 1 induces osteocytes to synthesize abundant FGF23 [30]; and tumor necrosis factor stimulates FGF23 levels in chronic kidney disease and non-renal inflammation [31]. In this study, the micro-circumstance of the metastasized lesion might have been able to induce MDA-MB-231 to secrete FGF23. In our previous report, the embryonic and infant stages of bone expressed abundant FGFR1 and αklotho, and FGF23 was produced mainly by osteoblastic cells rather than osteocytes in the embryonic stage [16]. However, as mice grow, FGF23-synthesizing cells were seen to chronologically shift from osteoblastic cells to osteocytes. Therefore, like the embryonic stage, the micro-circumstance of the metastatic lesion could have induced the ectopic synthesis of FGF23 in metastasized MDA-MB-231 cells.

More importantly, Kaludjerovic et al. stated that klotho in the bone is crucial for inducing FGF23 production upon renal failure [32]. In addition, Xiao et al. have consistently documented that klotho stimulates FGF23 expression in osteoblasts, leading to elevated Fgf23 expression in bone [33]. Fukumoto's team showed that FGF23-producing tumors caused TIO-expressed klotho in spindle-shaped cells in the tumor lesion [34]. In accordance with these reports, the current study demonstrated many FGFR1-immunoreactive fibroblastic stromal cells and some klotho-positive stromal cells in metastasized lesions, as well as elevated gene expression of FGFR1 in the metastasized femora. Therefore, we assume that FGF23 secreted by MDA-MB-231 cells may affect fibroblastic stromal cells in metastasized lesions. In particular, we speculate that FGF23 secreted by metastasized MDA-MB-231 cells would bind to FGFR1, forming a complex with klotho, which then accelerates FGF23 synthesis by MDA-MB-231 cells in the

metastasized lesion. This strongly suggests a positive feedback loop mediated by klotho and FGFR1 in a paracrine manner. However, in order to verify this possibility, we would need to conduct future work to clarify the cellular interaction between FGF23-synthesizing MDA-MB-231 cells and FGFR1-bearing fibroblastic stromal cells in the metastasized lesion.

In contrast to FGF23 synthesis by MDA-MB-231 cells, the reason for only osteocytes close to FGF23-secreting MDA-MB-231 cells being markedly inhibited for FGF23 synthesis still remains unknown. Even though FGF23 synthesis was inhibited, the osteocytes showed intense immunoreactivity of DMP-1, which is a predominant hallmark of osteocytes [35]. Therefore, we postulate that osteocytes close to FGF23-secreting MDA-MB-231 cells were selectively inhibited for FGF23 synthesis. Taken together, we could assume that FGF23 secreted by MDA-MB-231 cells but not by osteocytes may play a pivotal role in supporting and maintaining bone metastasis and its growth.

The serum concentration of FGF23 became 2.5 times higher in metastasized bone than in control specimens, and MDA-MB-231 cells in the metastasized lesion demonstrated broad and intense immunoreactivity of FGF23. However, the serum concentration of Pi was not significantly reduced in metastasized mice. Therefore, our findings seem to be of a different state from TIO [7-14], because the other long bones without tumor nests in the nu/nu mice did not show osteomalatic histology (*data not shown*). In addition, TIO may be caused by long-running secretin of FGF23, even though it is a small amount volume of FGF23 [12. 13].

Notably, no significant decrease in Pi occurred despite markedly elevated FGF23. Initially, we assumed that this contradictory phenomenon may be due to the fact that the FGF23 secreted by tumor cells is subjected to immediate processing at the C-terminus of

this molecule before reaching the kidney [33]. However, consistent with the elevated concentration of serum FGF23, the western blotting of FGF23 in the metastasized femora implies that the metastasized tumor cells abundantly secrete full-length FGF23. Therefore, the lack of significant change in serum Pi concentration may be because a reduced concentration of serum intact PTH may lead to the accelerated reabsorption of Pi in the kidney (presumably in the proximal tubules). It is likely that the increased CRE level, indicative of the reduced kidney function, may play a more central role in offsetting the phosphaturic effect of FGF23.

If so, it may raise the question of what the possible mechanism is for decreased kidney function. We hypothesize that one reason for the decreased kidney function in the metastasized mice is the cancer-associated kidney complications. Recently, it has been reported that both acute and chronic kidney diseases often occur in cancer patients [36]. The kidney diseases associated with cancer patients are caused by hypercalcemia, invasion of malignant tumors to the kidney, paraneoplastic glomerulopathy, chemotherapy, etc. Consistent with this report, the mice with bone metastasis in the current study may demonstrate elevated CRE concentrations that are indicative of decreased kidney function. Since FGF23 inhibits the synthesis of $1\alpha,25(OH)_2D_3$ by inhibiting 1α-hydroxylase in the kidney, the significantly-reduced serum levels of $1\alpha,25(OH)_2D_3$ that we detected do not seem surprising. However, it is ambiguous why the serum level of intact PTH was markedly reduced in mice with bone metastases. We postulate the following reasons for the reduction of intact PTH in our mice model: 1) Since MDA-MB-231 cells reportedly synthesize abundant PTHrP, the tumor-derived PTHrP may substitute for the biological action of intact PTH, 2) the slightly elevated calcium in mice with bone metastases may affect the synthesis of intact PTH, and 3) since

several researchers suggested that serum FGF23 directly regulates PTH secretion of the parathyroid cells [37, 38], the synthesis of FGF23 in MDA-MB-231 cells may affect the decreased serum concentration of intact PTH. However, these are merely our assumptions, and further examinations appear to be necessary.

Concluding Remarks

This study demonstrated that 1) MDA-MB-231 cells synthesized FGF23 during bone metastasis; 2) the osteocytes were inhibited from synthesizing FGF23 when they were closely surrounded by FGF23-secreting MDA-MB-231 cells, and 3) the immunoreactivity and gene expression of FGFR1 and αklotho were elevated in metastasized bone. Therefore, it is likely that FGF23 secreted by MDA-MB-231 cells plays a role in establishing suitable circumstances of metastasized lesion by mediating its receptor in an autocrine/paracrine fashion.

Acknowledgements

This study was partially supported by the Grants-in Aid for Scientific Research of Japan Society for the Promotion of Science (JSPS; Hasegawa T and Amizuka N) and Promoting International Joint Research (Bilateral Collaborations) of JSPS in Japan and NSFC in China (Amizuka N and Li M).

Conflict of interest

No potential conflicts of interest exist.

Authors' contribution

All authors contributed to the study conception and design. Yokoyama A is the main researcher who contributed to this work, including histochemical analyses. Hasegawa T, Yamada T, Hongo H, and Abe M under the guidance by Hiraga T performed animal experiments, such as preparation of cultured MDA-MB-231 cells, their injection into nu/nu mice, and fixation of the metastasized mice. Yimin and Yoshida T performed western blotting, and Imanishi Y and Yamamoto T conducted serum collection from mice, measurements of FGF23, and statistical analysis on serum concentration of calcium, Pi, and FGF23. Kuroshima S, Sasaki M, de Freitas PHL, Li M, Amizuka N, and Yamazaki Y participated in the discussion and preparation of the manuscript. Hasegawa T is the chief of this research project who organized collaborators and provided the whole outline of this experiment. The first draft of the manuscript was written by Hasegawa T and all authors have provided their inputs on the manuscript. All authors have read and approved the final manuscript.

References

1. Arguello F, Baggs RB and Frantz CN (1988) A murine model of experimental metastasis to bone and bone marrow. Cancer Res 48: 6876–6881.

2. Hiraga T, Nakajima T and Ozawa H (1995) Bone resorption induced by a metastatic

human melanoma cell line. Bone 16: 349–356.

3. Shimamura T, Amizuka N, Li M, Luiz de Freitas PH, White JH, Henderson JE, Shingaki S, Nakajima T and Ozawa H (2005) Histological observations on the microenvironment of osteolytic bone metastasis by breast carcinoma cell line. Biomed Res 26: 159–172.

4. Yoneda T, Sasaki A and Mundy GR (1994) Osteolytic bone metastasis in breast cancer. Breast Cancer Res Treat 32: 73–84.

5. Hiraga T (2019) Bone metastasis: Interaction between cancer cells and bone microenvironment. J Oral Biosci. 61(2): 95–98.

6. Seccareccia D (2010) Cancer-related hypercalcemia. Can Fam Physician 56: 244–246.

7. Shimada T, Muto T, Urakawa I, Yoneya T, Yamazaki Y, Okawa K, Takeuchi Y, Fujita T, Fukumoto S and Yamashita T (2002) Mutant FGF-23 responsible for autosomal dominant hypophosphatemic rickets is resistant to proteolytic cleavage and causes hypophosphatemia in vivo. Endocrinology 143: 3179–3182.

8. Yamazaki Y, Okazaki R, Shibata M, Hasegawa Y, Satoh K, Tajima T, Takeuchi Y, Fujita T, Nakahara K, Yamashita T and Fukumoto S (2002) Increased Circulatory Level of Biologically Active Full-Length FGF-23 in Patients with Hypophosphatemic Rickets/Osteomalacia. J Clin Endocrinol Metab 87: 4957–4960.

9. Folpe AL, Fanburg-Smith JC, Billings SD, Bisceglia M, Bertoni F, Cho JY, Econs MJ, Inwards CY, Jan de Beur SM, Mentzel T, Montgomery E, Michal M, Miettinen M, Mills SE, Reith JD, O'Connell JX, Rosenberg AE, Rubin BP, Sweet DE, Vinh TN, Wold LE, Wehrli BM, White KE, Zaino RJ and Weiss SW (2004) Most osteomalacia-associated mesenchymal tumors are a single histopathologic entity: an analysis of 32 cases and a comprehensive review of the literature. Am J Surg Pathol

28: 1–30.

10. Nasu T, Kurisu S, Matsuno S, Tatsumi K, Kakimoto T, Kobayashi M, Nakano Y, Wakasaki H, Furuta H, Nishi M, Sasaki H, Suzuki H, Ito N, Fukumoto S and Nanjo K. Tumor-induced hypophosphatemic osteomalacia diagnosed by the combinatory procedures of magnetic resonance imaging and venous sampling for FGF23. Intern Med. 2008;47(10):957–961.

11. Jiang Y, Xia WB, Xing XP, Silva BC, Li M, Wang O, Zhang HB, Li F, Jing HL, Zhong DR, Jin J, Gao P, Zhou L, Qi F, Yu W, Bilezikian JP and Meng XW (2012) Tumor-induced osteomalacia: an important cause of adult-onset hypophosphatemic osteomalacia in China: Report of 39 cases and review of the literature. J Bone Miner Res 27: 1967–1975.

12. Minisola S, Peacock M, Fukumoto S, Cipriani C, Pepe J, Tella SH and Collins MT (2017) Tumour-induced osteomalacia. Nat Rev Dis Primers. 3:17044. doi: 10.1038/nrdp.2017.44.

13. Kinoshita Y and Fukumoto S (2018) X-Linked hypophosphatemia and FGF23-related hypophosphatemic diseases: prospect for new treatment. Endocr Rev. 39(3):274–291.

14. Mansinho A, Ferreira AR, Casimiro S, Alho I, Vendrell I, Costa AL, Sousa R, Abreu C, Pulido C, Macedo D, Pacheco TR, Correia L and Costa L (2019) Levels of circulating fibroblast growth factor 23 (FGF23) and prognosis in cancer patients with bone metastases. Int J Mol Sci 20(3). pii: E695. doi: 10.3390/ijms20030695

15. Ubaidus S, Li M, Sultana S, Luiz de Freitas PH, Oda K, Maeda T, Takagi R and Amizuka N (2009) FGF23 is mainly synthesized by osteocytes in the regularly distributed osteocytic lacunar canalicular system established after physiological bone remodeling. J Electron Microsc (Tokyo) 58: 381–392.

16. Sakurai A, Hasegawa T, Kudo A, Shen Z, Nagai T, Abe M, Yoshida T, Hongo H, Yamamoto T, Yamamoto T, Oda K, Freitas PHL, Li M, Sano H and Amizuka N (2017) Chronological immunolocalization of sclerostin and FGF23 in the mouse metaphyseal trabecular and cortical bone. Biomed Res 38(4): 257–267.

17. Nabeshima Y (2006) Toward a better understanding of Klotho. Sci Aging Knowledge Environ 8: pe11. doi: 10.1126/sageke.2006.8.pe11

18. Urakawa I, Yamazaki Y, Shimada T, Iijima K, Hasegawa H, Okawa K, Fujita T, Fukumoto S and Yamashita T (2006) Klotho converts canonical FGF receptor into a specific receptor for FGF23. Nature 444: 770–777.

19. Nakatani T, Sarraj B, Ohnishi M, Densmore MJ, Taguchi T, Goetz R, Mohammadi M, Lanske B and Razzaque MS (2009) In vivo genetic evidence for klotho-dependent, fibroblast growth factor 23 (Fgf23)-mediated regulation of systemic phosphate homeostasis. FASEB J 23: 433–441.

20. Fukumoto S (2009) The role of bone in phosphate metabolism. Mol Cell Endocrinol. 310(1-2): 63–70.

21. Hasegawa T, Sasaki M, Yamada T, Ookido I, Yamamoto T, Hongo H, Yamamoto T, Oda K, Yokoyama K and Amizuka N (2013) Histochemical examination of vascular medial calcification of aorta in klotho-deficient mice. J Oral Biosci 55: 10–15.

22. Hasegawa T, Yamamoto T, Sakai S, Miyamoto Y, Hongo H, Qiu Z, Abe M, Takeda S, Oda K, de Freitas PHL, Li M, Endo K and Amizuka N (2019) Histological effects of the combined administration of eldecalcitol and a parathyroid hormone in the Metaphyseal Trabeculae of Ovariectomized Rats. J Histochem Cytochem 67(3): 169–184.

23. Hasegawa T, Endo T, Tsuchiya E, Kudo A, Shen Zhao, Moritani Y, Abe M, Yamamoto T, Hongo H, Tsuboi K, Yoshida T, Nagai T, Khadiza N, Yokoyama A,

Luiz de Freitas PH, Li M and Amizuka N (2017) Biological application of focus ion beam-scanning electron microscopy (FIB-SEM) to the imaging of cartilaginous fibrils and osteoblastic cytoplasmic processes. J Oral Biosci 59: 55–62.

24. Hu X, Du S, Yu J, Yang X, Yang C, Zhou D, Wang Q, Qin S, Yan X, He L, Han D and Wan C (2016) Common housekeeping proteins are upregulated in colorectal adenocarcinoma and hepatocellular carcinoma, making the total protein a better "housekeeper". Oncotarget. 7:66679-66688.

25. Nie X, Li C, Hu S, Xue F, Kang YJ and Zhang W (2017) An appropriate loading control for western blot analysis in animal models of myocardial ischemic infarction. Biochem Biophys Rep. 12:108-113.

26. Yamamoto T, Hasegawa T, Sasaki M, Hongo H, Tsuboi K, Shimizu T, Ota M, Haraguchi M, Takahata M, Oda K, Luiz de Freitas PH, Takakura A, Takao-Kawabata R, Isogai Y and Amizuka N (2016) Frequency of Teriparatide Administration Affects the Histological Pattern of Bone Formation in Young Adult Male Mice. Endocrinology 157: 2604–2620.

27. Imanishi Y, Hashimoto J, Ando W, Kobayashi K, Ueda T, Nagata Y, Miyauchi A, Koyano HM, Kaji H, Saito T, Oba K, Komatsu Y, Morioka T, Mori K, Miki T and Inaba M (2012) Matrix extracellular phosphoglycoprotein is expressed in causative tumors of oncogenic osteomalacia. J Bone Miner Metab 30: 93–99.

28. Ito N, Wijenayaka AR, Prideaux M, Kogawa M, Ormsby RT, Evdokiou A, Bonewald LF, Findlay DM and Atkins GJ (2015) Regulation of FGF23 expression in IDG-SW3 osteocytes and human bone by pro-inflammatory stimuli. Mol Cell Endocrinol 399: 208–218.

29. Bär L, Feger M, Fajol A, Klotz LO, Zeng S, Lang F, Hocher B and Föller M (2018) Insulin suppresses the production of fibroblast growth factor 23 (FGF23). Proc Natl Acad Sci USA 115(22):5804–5809.

30. Kamiya N, Yamaguchi R, Aruwajoye O, Kim AJ, Kuroyanagi G, Phipps M, Adapala

NS, Feng JQ and Kim HK (2017) Targeted disruption of NF1 in osteocytes increases FGF23 and osteoid with osteomalacia-like bone phenotype. J Bone Miner Res 32(8): 1716–-1726.

31. Egli-Spichtig D, Imenez Silva PH, Glaudemans B, Gehring N, Bettoni C, Zhang MYH, Pastor-Arroyo EM, Schönenberger D, Rajski M, Hoogewijs D, Knauf F, Misselwitz B, Frey-Wagner I, Rogler G, Ackermann D, Ponte B, Pruijm M, Leichtle A, Fiedler GM, Bochud M, Ballotta V, Hofmann S, Perwad F, Föller M, Lang F, Wenger RH, Frew I and Wagner CA (2019) Tumor necrosis factor stimulates fibroblast growth factor 23 levels in chronic kidney disease and non-renal inflammation. Kidney Int 96(4): 890–905.

32. Kaludjerovic J, Komaba H, Sato T, Erben Rg, Baron R, Olauson H, Larsson TE and Lanske B (2017) Klotho expression in long bones regulates FGF23 production during renal failure. FASEB J 31: 2050–2064

33. Xiao Z, King G, Mancarella S, Munkhsaikhan U, Cao L, Cai C and Quarle LD (2019) FGF23 expression is stimulated in transgenic α-Klotho longevity mouse model. JCI Insight 4: e132820

34. Kinoshita Y, Takashi Y, Ito N, Ikegawa S, Mano H, Ushiku T, Fukayama M, Nangaku M and Fukumoto S (2018) Ectopic expression of Klotho in fibroblast growth factor 23 (FGF23)-producing tumors that cause tumor-induced rickets/osteomalacia (TIO). Bone Rep 10:100192. doi: 10.1016/j.bonr.2018.100192.

35. Toyosawa S, Shintani S, Fujiwara T, Ooshima T, Sato A, Ijuhin N and Komori T (2001) Dentin matrix protein 1 is predominantly expressed in chicken and rat osteocytes but not in osteoblasts. J Bone Miner Res 16: 2017–2026.

36. Kitai Y, Matsubara T and Yanagita M (2015) Onco-nephrology: current concepts and future perspectives. Jpn J Clin Oncol. 45:617-628.

37. Ben-Dov IZ, Galitzer H, Lavi-Moshayoff V, Goetz R, Kuro-o M, Mohammadi M, Sirkis R, Naveh-Many T and Silver J (2007) The parathyroid is a target organ for FGF23 in rats. J Clin Invest. 117：4003–4008.

38. Olauson H, Lindberg K, Amin R, Sato T, Jia T, Goetz R, Mohammadi M, Andersson G, Lanske B and Larsson TE (2013) Parathyroid-specific deletion of klotho unravels a novel calcineurin-dependent FGF23 signaling pathway that regulates PTH secretion. PLoS Genet. 9:e1003975.

Figure Legends

Fig. 1

Radiograph and histology of the femora in nu/nu mice bearing bone-metastasized MDA-MB-231 cells

Soft X-ray analysis demonstrates the translucent areas representing osteolytic metastases in the distal metaphyses of the femora and proximal metaphyses of the tibiae (**a**, white arrows in an inset). H-E staining shows a large tumor nest of MDA-MB-231 cells and few trabeculae in the femoral metastasized lesion **(b)**. In the metastatic lesion, many TRAP-positive osteoclasts (red color) are located on the scalloped bone surface intensely positive for osteopontin immunoreactivity (brown color, white arrows in **d**) (**c** and **d)**. Panel **d** is a highly magnified image of **c**. tb: trabecula; BM: bone marrow

Bars, **a**: 1 cm, **b**: 500 μm, **c**: 30 μm, **d**: 20 μm

Fig. 2

Immunohistochemistry of FGF23 in bone-metastasized MDA-MB-231 cells in the

femoral metaphyses

The metastasized tumor nests in the femora display intense FGF23 immunoreactivity (brown, **a**). Panel **b** is a highly magnified image of the boxed area in **a**. Note that osteocytes (ocy) surrounded by FGF23-positive tumor cells do not exhibit FGF23 immunoreactivity (**b**). However, many osteocytes distant from the tumor nest exhibit apparent immunoreactivity of FGF23 (**c**). Western blotting detects higher intensity of full-length FGF23 expression (32 kDa) in the femora with metastasized MDA-MB-231 cells compared to the control femora (**d)**. The index of FGF23 protein expression is about 3.6-fold higher in the femora with metastasized MDA-MB-231 cells relative to the control femora (**e**). Panel **f** shows the gel staining images of total protein in the control femora and the femora with metastasized MDA-MB-231 cells as the loading control. There was no significant difference between the intensity of total protein in the control femora and the femora with metastasized MDA-MB-231 cells (**g**).

tb: trabecula, ocy: osteocyte, BM: bone matrix

Bars, **a**: 250 μm, **b, c**: 50 μm

Fig. 3

Immunohistochemistry of FGF23 in bone-metastasized MDA-MB-231 cells in femoral cortical bone

Panels **a** and **b** are low-magnified images of immunodetection of FGF23 and DMP-1 (brown). Osteocytes in the cortical bone close to the FGF23-positive tumor nests (above the dotted line) do not appear positive for FGF23, whereas osteocytes below the dotted lines show FGF23 immunopositivity. In contrast, DMP-1 positivity can be seen in all

osteocytes in the cortical bone regardless of the distance from the tumor nest (note that the osteocytes both above and below the dotted line are DMP-1-positive). Panels **c** and **d** are higher magnified images of the cortical bone adjacent to the tumor nest. No osteocytes show FGF23 (**c**), but all osteocytes display DMP-1 immunoreactivity (**d**). In a distant region from the tumor nest, osteocytes reveal immunopositivity for both FGF23 (**e**) and DMP-1 (**f**).

Bars, **a**, **b**: 50 μm, **c**–**f**: 30 μm

Fig. 4

Statistical analyses on serum concentration of Ca, Pi, FGF23, intact PTH, 1*α*,25(OH)$_2$D$_3$, and CRE in mice

The concentrations of serum FGF23 are 156 ± 18 pg/mL, 386 ± 59 pg/mL, and 230 ± 9 pg/mL in control mice, mice with bone metastases, and mice with subcutaneous injections of MDA-MB-231 cells in the region of the mammary glands, respectively (**a**). There are significant differences between control mice and mice with bone metastases as well as between mice with bone metastases and mice injected with MDA-MB-231 cells in the mammary glands. Serum Pi (**b**) and calcium (**c**) do not show significant differences between groups. Intact PTH and 1α,25(OH)$_2$D$_3$ levels are significantly lower in mice with bone metastases than in control mice (**d** and **e**), while CRE levels in mice with bone metastases are significantly higher than those in control mice (**f**).

Fig. 5

The immunolocalization of FGFR1 and αklotho in the metastasized femora and the immunolocalization of FGF23, FGFR1, and αklotho in the cultured MDA-MB231 cells and mammary glands injected with MDA-MB-231 cells

Fibroblastic stromal cells (white arrowheads in **a** and **b**) but not cuboidal tumor cells (black arrows in **a** and **b**) of metastasized tumor nests are positive for FGFR1 (brown color; panels **a** and **b** are obtained from the central and peripheral region of the metastasized lesion, respectively). Fibroblastic stromal cells also exhibit faint αklotho immunoreactivity (see faint brown color in fibroblastic stromal cells as indicated by black arrows in the inset in panel **c**). Panels **d**–**f** show the immunohistochemistry of FGF23, FGFR1, and αklotho in the mammary glands after the subcutaneous injection of MAD-MB-231 cells, whereas panels **g**–**i** demonstrate the immunohistochemistry of FGF23, FGFR1, and αklotho in cultured MAD-MB-231 cells. See accumulated tumor cells without obvious immunoreactivity of FGF23, FGFR1, and αklotho (brown color, **d**–**f**). Immunohistochemistry of FGFR1 and αklotho also demonstrate no immunoreaction in cultured MAD-MB-231 cells (**h** and **i**). In contrast, cultured MDA-MB-231 cells show very faint FGF23 immunoreactivity (brown) (**g**). Note no immunoreactivity (arrows) and faint immunopositivity (arrowheads) for FGF23 in MDA-MB-231 cells.

Bars: **a**–**c**: 50 μm, **d**–**f**: 30 μm, **g**–**i**: 20 μm

Fig. 6

Gene expression of *Fgf23, Fgfr1* and *αKlotho* in control and metastasized femora and control and MDA-MB-231 cell-injected mammary glands

Panels **a** and **b** show the gene expression of *Fgf23, Fgfr1, and αKlotho* in the control and

metastasized femora (**a**: real-time PCR, **b**: RT-PCR), while panel **c** and **d** depict the gene expression of *Fgf23, Fgfr1, and αKlotho* in the control and MDA-MB-231 cell-injected mammary glands (**c**: real-time PCR, **d**: RT-PCR). In the metastasized femora, the gene expression of *Fgfr1* is significantly increased compared to the control femora (**a, b**). Both *Fgf23* and *αKlotho* gene expression are comparable between the control and metastasized femora (**a, b**). Note that gene levels of *Fgfr1* and *αKlotho* are significantly decreased in the MDA-MB-231 cell-injected mammary glands compared to the control mammary glands (**c, d**). There is no significant difference in *Fgf23* between the control and MDA-MB-231 cell-injected mammary glands.

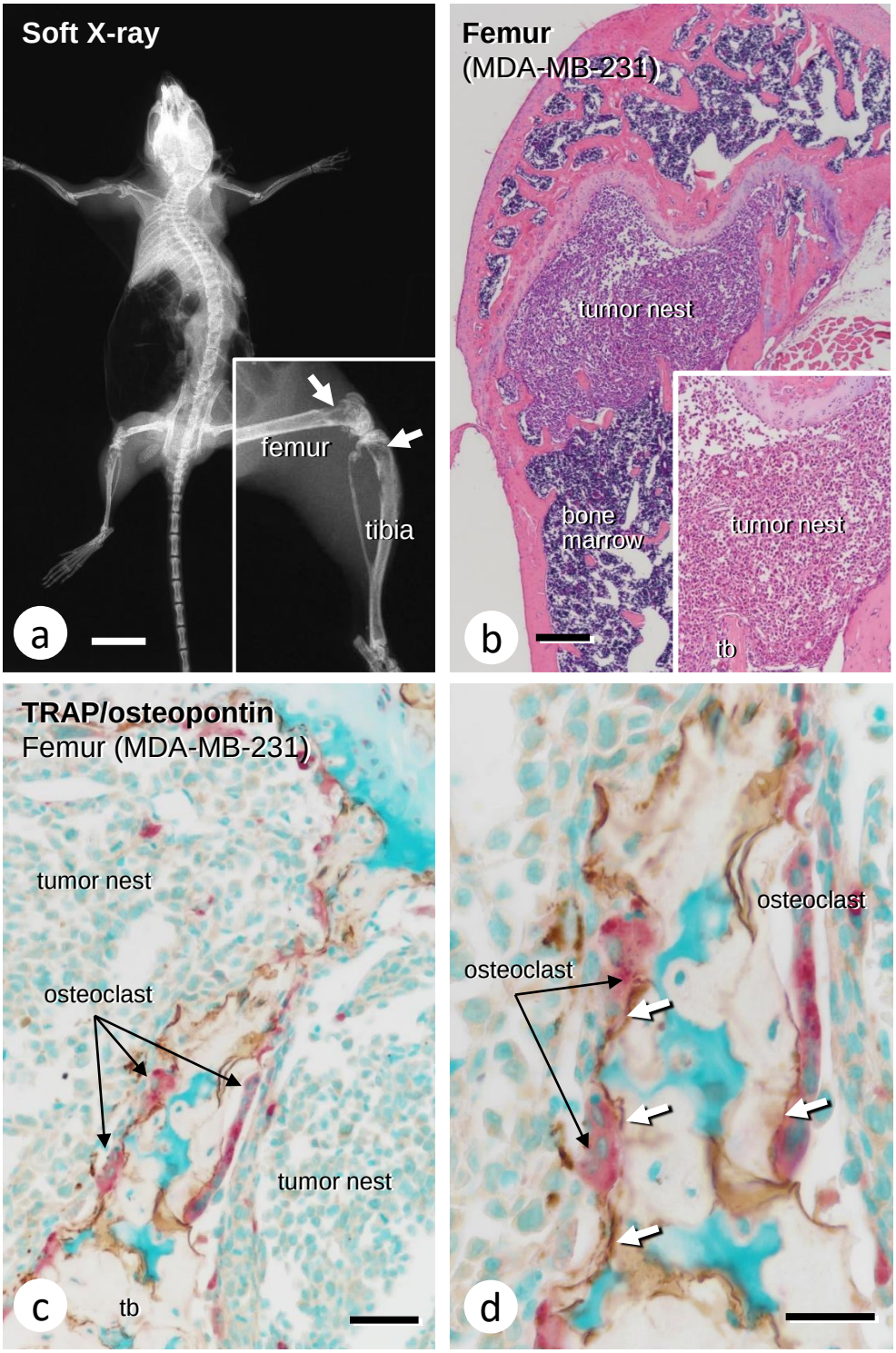
Soft X-ray
femur
tibia
a
Femur
(MDA-MB-231)
tumor nest
bone
marrow
tumor nest
tb
b
TRAP/osteopontin
Femur (MDA-MB-231)
tumor nest
osteoclast
tumor nest
tb
c
osteoclast
osteoclast
d

Fig. 1

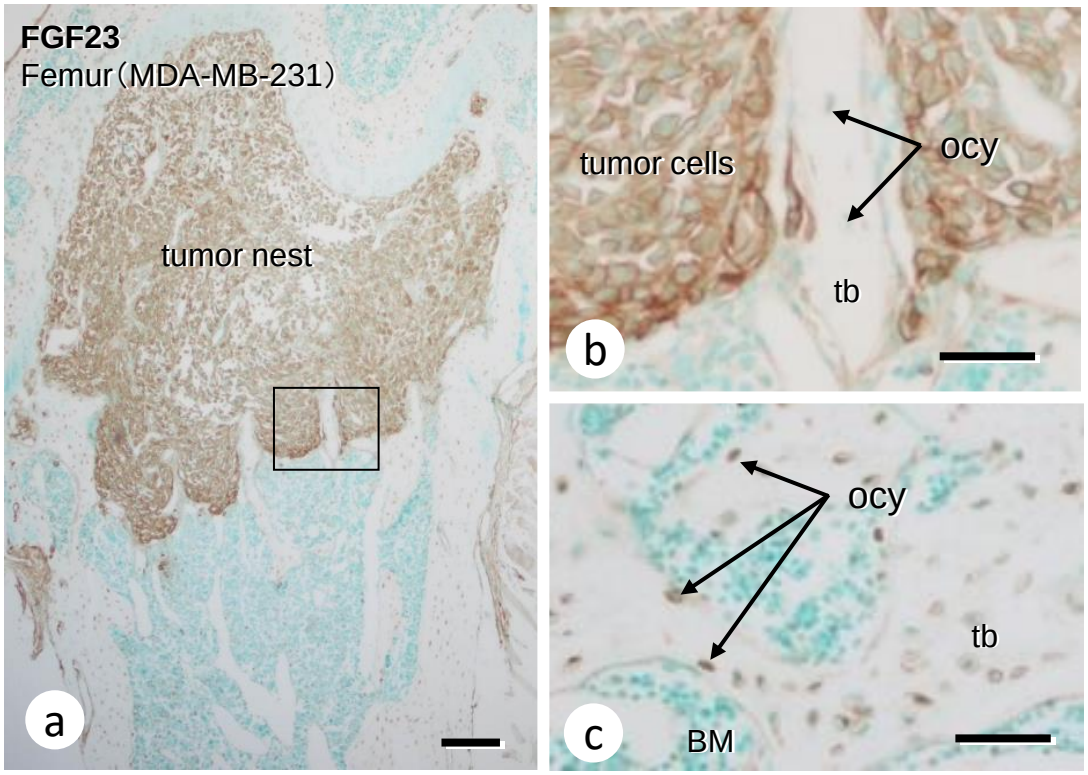
FGF23
Femur（MDA-MB-231）
tumor nest
a
tumor cells
ocy
tb
b
ocy
tb
BM
c

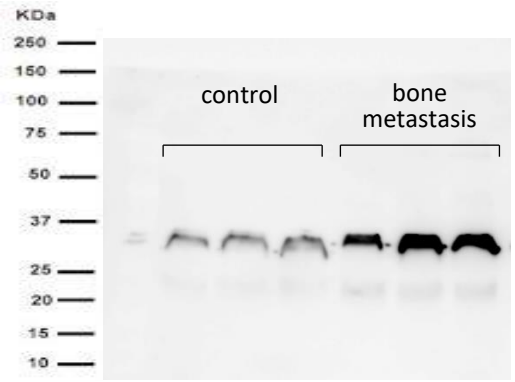
KDa
250
150
100
75
50
37
25
20
15
10
control
bone metastasis

d

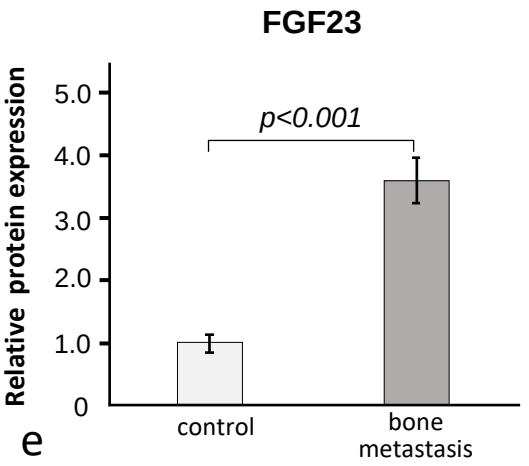
FGF23
Relative protein expression
5.0
4.0
3.0
2.0
1.0
0
p<0.001
control
bone metastasis

e

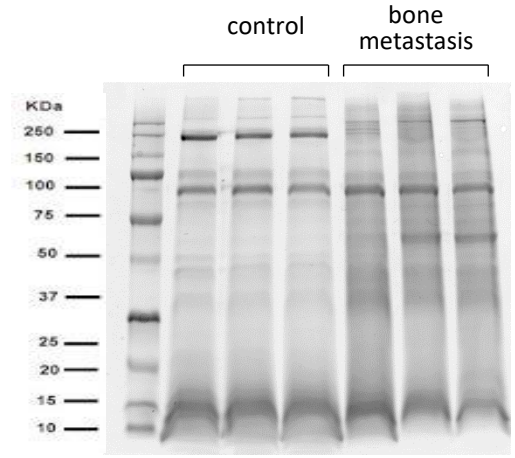
control
bone metastasis
KDa
250
150
100
75
50
37
25
20
15
10

f

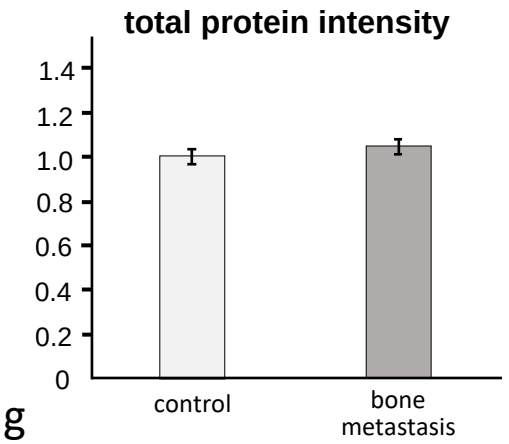
total protein intensity
1.4
1.2
1.0
0.8
0.6
0.4
0.2
0
control
bone metastasis

g

Fig. 2

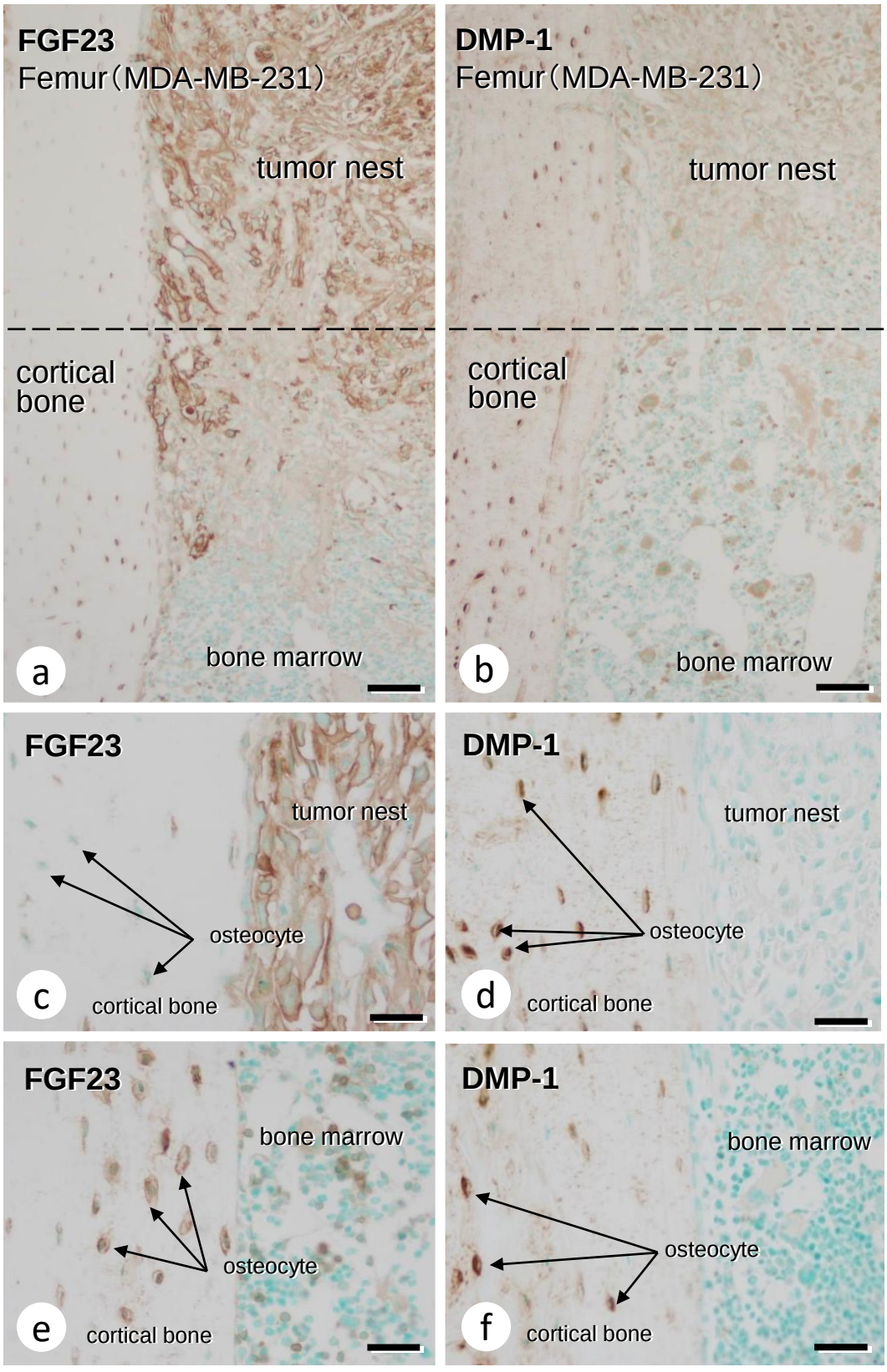
FGF23
Femur（MDA-MB-231）
tumor nest
cortical bone
bone marrow
a
DMP-1
Femur（MDA-MB-231）
tumor nest
cortical bone
bone marrow
b
FGF23
tumor nest
osteocyte
cortical bone
c
DMP-1
tumor nest
osteocyte
cortical bone
d
FGF23
bone marrow
osteocyte
cortical bone
e
DMP-1
bone marrow
osteocyte
cortical bone
f

Fig. 3

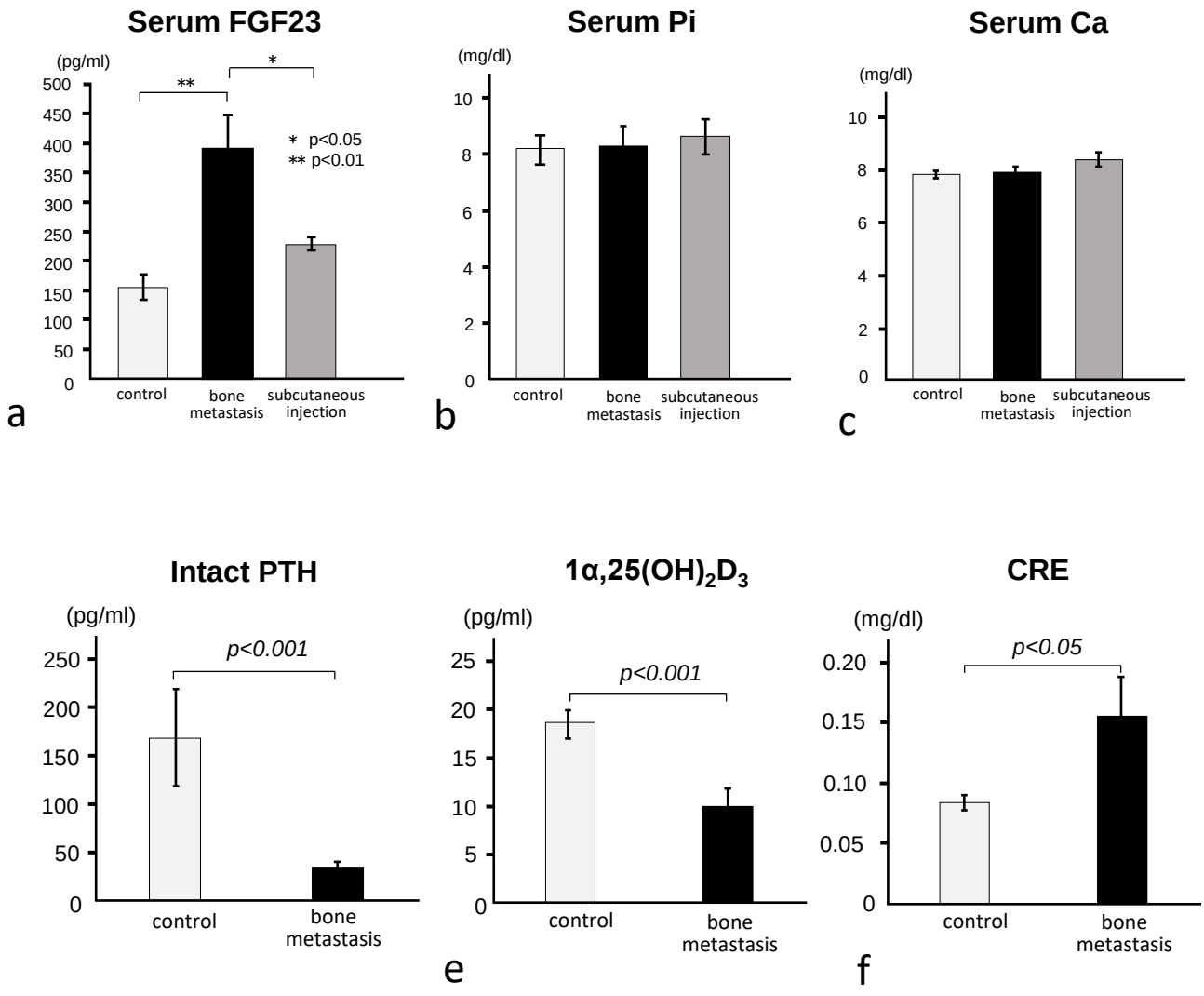
Serum FGF23
(pg/ml)
500
450
400
350
300
250
200
150
100
50
0
**
*
* p<0.05
** p<0.01
control
bone metastasis
subcutaneous injection
a
Serum Pi
(mg/dl)
10
8
6
4
2
0
control
bone metastasis
subcutaneous injection
b
Serum Ca
(mg/dl)
10
8
6
4
2
0
control
bone metastasis
subcutaneous injection
c
Intact PTH
(pg/ml)
250
200
150
100
50
0
p<0.001
control
bone metastasis
d
1α,25(OH)2D3
(pg/ml)
25
20
15
10
5
0
p<0.001
control
bone metastasis
e
CRE
(mg/dl)
0.20
0.15
0.10
0.05
0
p<0.05
control
bone metastasis
f

Fig. 4

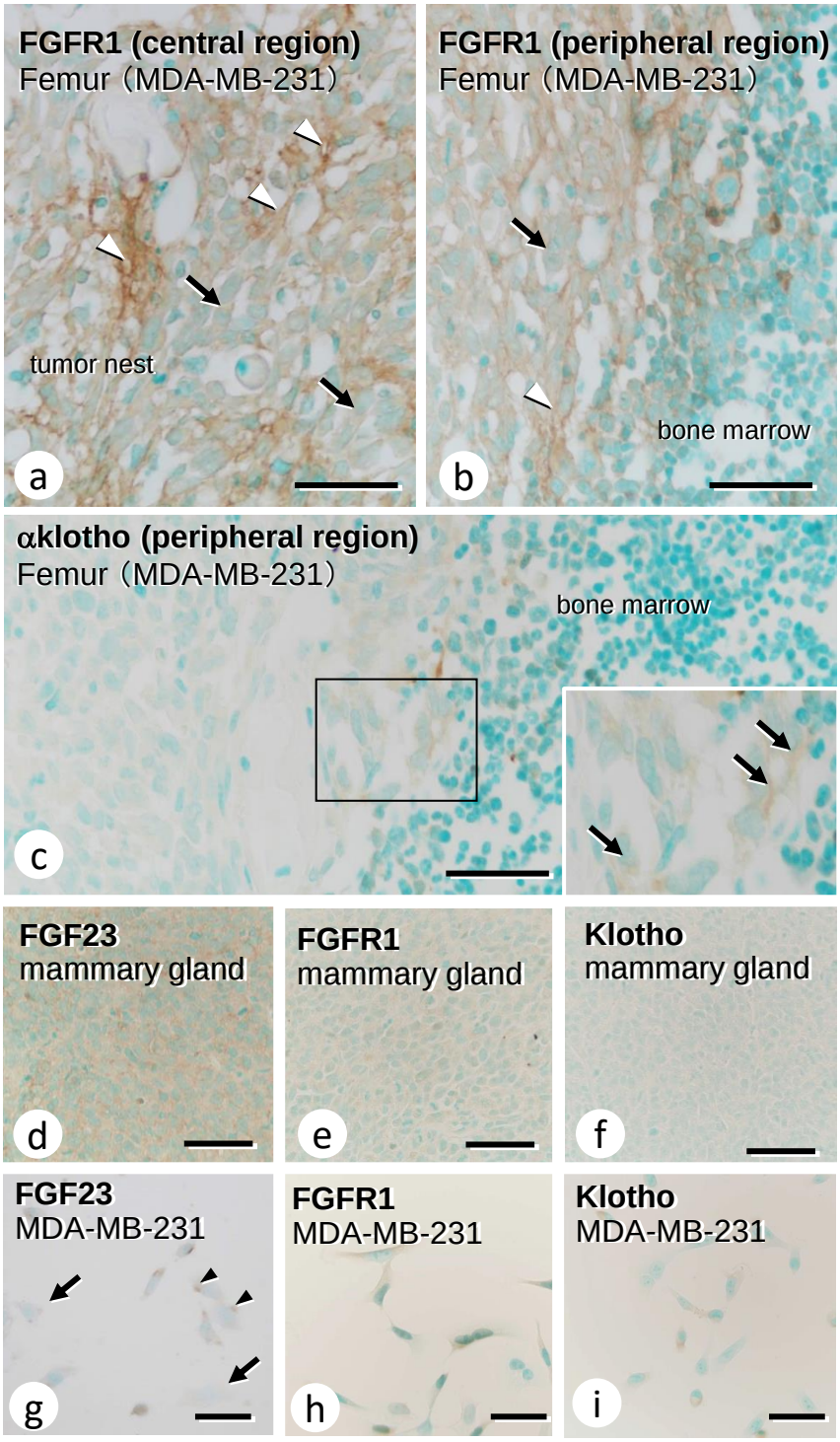
FGFR1 (central region)
Femur（MDA-MB-231）
tumor nest
a
FGFR1 (peripheral region)
Femur（MDA-MB-231）
bone marrow
b
αklotho (peripheral region)
Femur（MDA-MB-231）
bone marrow
c
FGF23
mammary gland
d
FGFR1
mammary gland
e
Klotho
mammary gland
f
FGF23
MDA-MB-231
g
FGFR1
MDA-MB-231
h
Klotho
MDA-MB-231
i

Fig. 5

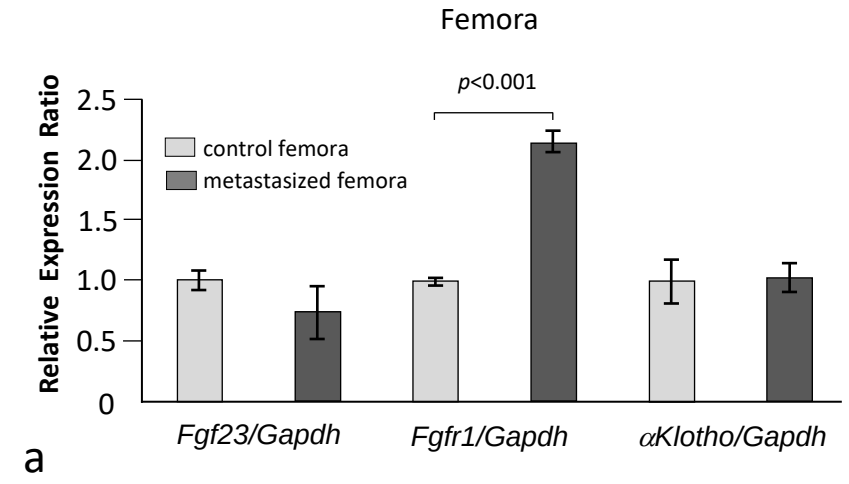
Femora
p<0.001
Relative Expression Ratio
2.5
2.0
1.5
1.0
0.5
0
control femora
metastasized femora
Fgf23/Gapdh
Fgfr1/Gapdh
αKlotho/Gapdh

a

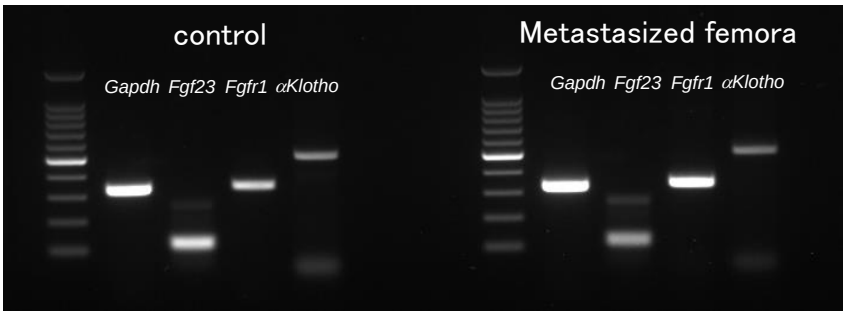
control
Gapdh Fgf23 Fgfr1 αKlotho
Metastasized femora
Gapdh Fgf23 Fgfr1 αKlotho

b

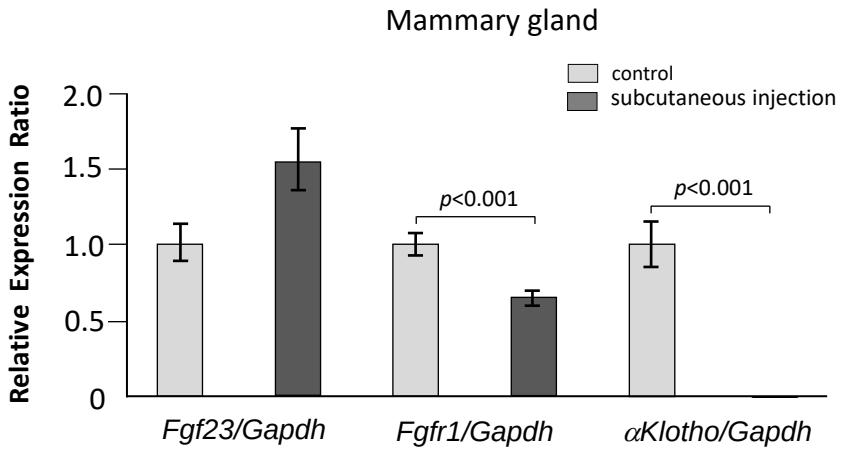
Mammary gland
control
subcutaneous injection
Relative Expression Ratio
2.0
1.5
1.0
0.5
0
p<0.001
p<0.001
Fgf23/Gapdh
Fgfr1/Gapdh
αKlotho/Gapdh

c

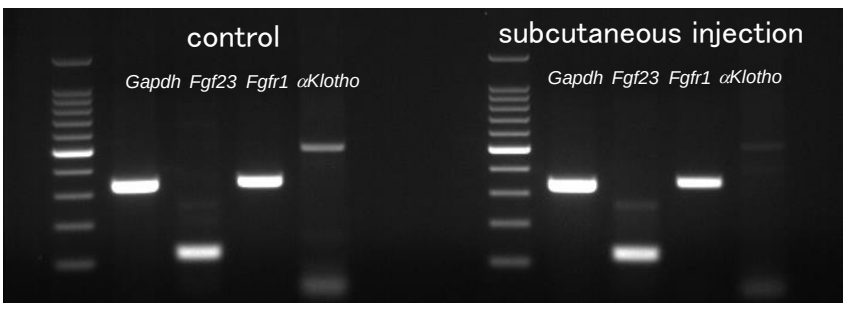
control
Gapdh Fgf23 Fgfr1 αKlotho
subcutaneous injection
Gapdh Fgf23 Fgfr1 αKlotho

d

Fig. 6